Int. J. Electrochem. Sci., 14 **(2019)** 4838 – 4851, doi: 10.20964/2019.05.61

International Journal of
ELECTROCHEMICAL
SCIENCE
www.electrochemsci.org

Effect of CO_2 and H_2S on the Corrosion Resistance of FV520B Steel in Salinity Water

Ming Liu[1,*], *Sheji Luo*[2,*], *Hui Zhang* [2], *Han Chen*[3]

[1] State Key Laboratory for Strength and Vibration of Mechanical Structures, Xi'an Jiaotong University, Xi'an 710049, PR China 1; liuming0313@xjtu.edu.cn
[2] School of Materials Science and Engineering, Xi'an Shiyou University, Xi'an 710065, PR China 2; sjluo@xsyu.edu.cn
[3] Technical Monitoring Center of Changqing Oilfield Company, Xi'an 710018, PR China 3;
[*]E-mail: liuming0313@xjtu.edu.cn (M.L.); sjluo@xsyu.edu.cn (S.L.)

Received: 3 February 2019 / *Accepted:* 11 March 2019 / *Published:* 10 April 2019

The corrosion behavior of FV520B stainless steel in different salinity water was studied by electrochemical measurements such as potentiodynamic polarization, electrochemical impedance spectroscopy (EIS), cyclic voltammetry (CV) and X−ray photoelectron spectroscopy (XPS). The results showed that the open circuit potential (OCP) shifts negatively and the thermodynamic stability of FV520B steel decreases when CO_2 and H_2S were introduced into the salinity water (SW). The polarization curves of FV520B steel show typical passive characteristics in the salinity solutions. When CO_2 and H_2S are introduced into the SW, the corrosion current density of FV520B steel increases, the polarization resistance decreases, and the corrosion resistance decreases, and the corrosion resistance is the poorest in H_2S salinity water. XPS analysis shows that the passive film of FV520B steel are mainly consist of oxides and hydroxides of Fe, Cr, Mo, Ni and Cu. With the introducing of CO_2 and H_2S, the content of $Fe^{2+}$and Cr^{3+} in passive film decreases, the content of Fe^{3+} and Cr^{6+} increases, and the corrosion resistance of passive film decreases. The corrosion resistance of FV520B steel in SW is significantly reduced by corrosive gas CO_2 and H_2S, and the corrosion resistance in H_2S shows the worst.

Keywords: FV520B; corrosion; hydrogen sulfide; cyclic voltammetry; XPS

1. INTRODUCTION

As the core component of centrifugal compressor, the service life of blade directly affects the overall performance of compressor. Because of the complex force on blade and the bad working environment, corrosion, fatigue and stress corrosion cracking often occur [1−3]. On the basis of Cr13 stainless steel, FV520B was developed by adding Mo, Ti, Nb, Cu and other strengthening elements. Because of excellent comprehensive properties such as high strength, high toughness, good weld ability

and corrosion resistance, FV520B steel has been widely used in the manufacturing of impeller of circulating hydrogen compressor and become the main structural material for manufacturing centrifugal compressor blades [4−6].

In the petroleum and natural gas industry, H_2S and CO_2 are the main corrosive gases in oil and gas fields. H_2S and CO_2 corrosion are common serious problems in the process of exploitation, transportation and refining [7,8]. During the working process of centrifugal compressor, the blades of centrifugal compressor often contact with corrosive media such as H_2S, CO_2 and Cl^- etc. Corrosion has become a prominent problem threatening the safety of centrifugal compressor. The microstructure and mechanical properties, fracture mechanisms and stress corrosion cracking behaviors of FV520B have been deeply studied by scholars at home and abroad [9−12], and some achievements have been reached. However, the study on corrosion behavior of FV520B steel is relatively few, especially the electrochemical and passive behavior of FV520B steel in the salinity solution containing H_2S or CO_2 has not been in-depth studied.

Therefore, the corrosion behavior of FV520B steel in the environment of SW, SW+CO_2, SW +H_2S were studied by electrochemical testing method and X−ray photoelectron spectroscopy. The relevant electrochemical parameters were obtained, the corrosion mechanisms were analyzed. The research results could have important theoretical significance and engineering application values for the safe use of fan impellere.

2. EXPERIMENTAL

2.1. Materials and solution

In this work, FV520B martensite precipitation hardening stainless steel was used for the experiments, the chemical composition are C 0.066, Si 0.057, Mn 0.766, S0.0024, Cr 13.71, Mo 1.301, Ni 4.508, Cu 0.995, Co 0.023, Ti 0.050, V 0.084, and Fe balance (in % by mass). Samples for electrochemical tests had dimensions of 10 mm×10 mm×3 mm, the exposed measurement area was 10 mm× 10 mm, which was retained by epoxy resin. Prior to the experiment, the samples were polished with silicon carbide water polishing papers down to 2000#. Then, the samples were ultrasonically cleaned in acetone and rinsed in distilled water.

The salinity water (SW) was chosen to simulate the base actual working condition. The salinity water was prepared by diluting 0.865 g $CaCl_2$, 0.5085 g $MgCl_2$, 2.635 g Na_2SO_4 and 5.915 g NaCl with distilled water to a total volume of 1 liter with the pH of 6.8. Three kinds of solutions were used in the test: SW, SW+CO_2, and SW+H_2S. CO_2, and H_2S gases were introduced into the SW. The partial pressure of CO_2 and H_2S were 0.83 kPa and the amount of gases inflow were several bubbles per minute. Before testing, the pH value of the solution after bubbling was tested, and the pH value of the solution was approximately 4.3 for H_2S, and 5.6 for CO_2. The gases were continuously introduced until the tests were ended.

2.2. Electrochemical measurements

Electrochemical tests were performed using the PARSTAT 2273 electrochemical workstation. A three−electrode system was applied, with FV520B steel serving as the working electrode, the saturated calomel electrode (SCE) as the reference electrode, and a platinum gauge as the counter electrode. The electrochemical test were measured before the samples immersed in test solutions for 0.5 h. Potentiodynamic polarization curves were measured from −250 mV (Vs. OCP) to the potential where the anodic current density attained 1 $mA \cdot cm^{-2}$, with a scanning rate of 1 $mV \cdot s^{-1}$. Cyclic voltammetry curves were measured from −500 mV_{SCE} to 400 mV_{SCE} bese on the testing results of polarization curves, with a scanning rate of 50 $mV \cdot s^{-1}$. EIS tests were performed at OCP with a scanning range of 100 kHz –10 mHz at the amplitude of 10 mV, and the results were analyzed with ZsimpWin Software. All tests were conducted at ambient temperature (25±1 °C). Each test was performed thrice to ensure the repetitiveness of the results.

2.3. XPS analysis

The passive film compositions of FV520B steel formed in different salinity solutions for 1 day were analyzed by Kratos AXIS Ultra DLD X−ray photoelectron spectroscopy (XPS). The monochromator was Al Ka, the sensitivity was 100 kcps, the scanning range of energy spectrum was 0−1350 eV, the scanning spacing was 1 eV, and the narrow scanning spacing was 0.1 eV. The energy spectrum was corrected by C1s (285.0 eV). Element composition and content were analyzed by comparing with standard spectra. Standard data were obtained from Perkin−Elmer's XPS data manual and XPS International Inc. website. The Xpspeak 4.1 was used to analyze the data by Gauss−Newton fitting method.

3. RESULTS AND DISCUSSION

3.1. OCP−time measurements

Figure 1 shows OCP of FV520B steel after immersion in different salinity solutions (SW, SW+CO_2 and SW+H_2S) for 0.5 h. It can be seen that the OCP of FV520B steel shifts positively with the increasing of the corrosion time. The OCP tends to be stable after 0.5 h immersion. The OCP of the samples are −0.259 V_{SCE}, −0.282 V_{SCE} and −293 V_{SCE} for FV520B steel immersion in SW, SW+CO_2 and SW+H_2S, respectively. Comparing the OCP of samples in different environments, it can be found that the OCP of FV520B steel samples shifted negatively when CO_2 and H_2S were introduced into the SW, and the thermodynamic stability of FV520B steel decreased. OCP is the coupling potential of anodic and cathodic reactions on the surface of steel [13]. Thermodynamic stability of electrochemical corrosion of steel can be preliminarily judged from OCP, which decreases with the decreasing of corrosion potential. The order of thermodynamic stability of FV520B steel in three test solutions are: SW >SW+ CO_2 >SW+ H_2S.

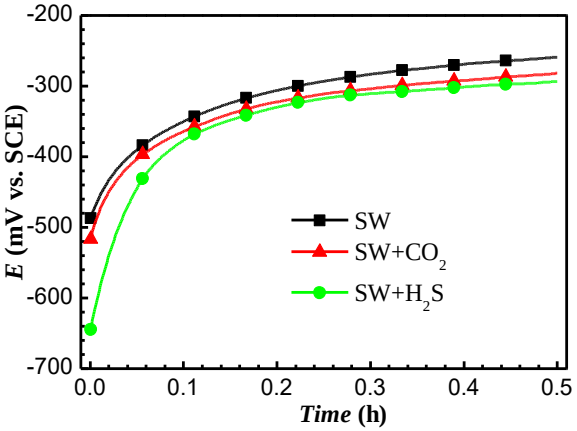

Figure 1. OCP of FV520B steel after immersion in different salinity solutions.

3.2. Electrochemical impedance spectroscopy

The EIS diagrams of FV520B steel after immersion in different salinity solutions are displayed in Fig. 2. It can be seen in Fig. 2(a) that Nyquist plots of steel are incomplete semicircle. The Bode diagrams with a wide phase angle in Fig. 2(b) indicate that there are at least two time constants [14−16]. The low frequency capacitance and impedance arcs are related to the double layer capacitance and charge transfer resistance. The radius of the impedance arc decreased with the CO_2 and H_2S introducing into the SW, which indicates that the corrosion degree of the steel increases with the existing of corrosive gases.

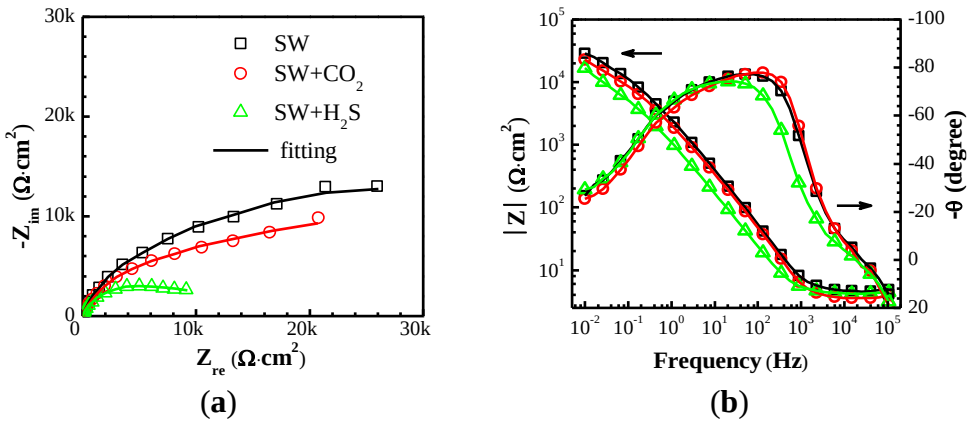

Figure 2. The diagrams of FV520B steel after immersion in different salinity solutions: (a) Nyquist; (b) Bode.

The two time constants equivalent circuit in Fig. 3 was used to to fit the EIS data [14−16], where R_s is the solution resistance, R_{ct} is the charge transfer resistance, Q_{dl} is the double layer capacitance of reaction interface, Q_f is the capacitance of corrosion product film, R_f is the resistance of the corrosion product film. The fitting line are also plotted in Fig. 2, and the fitting results are very consistent with the experimental results indicating the feasible of the equivalent circuit.

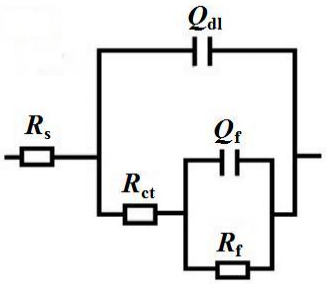

Figure 3. Equivalent circuit of FV520B steel after immersion in different salinity solutions.

The fitting results of the EIS parameters of FV520B steel after immersion in different salinity solutions are listed in Table 1. It can be seen that R_s changes little ranging from 2−5 $\Omega \cdot cm^2$; R_{ct} is between 508−1360 $\Omega \cdot cm^2$, and R_f is at 12.44−41.86 $k\Omega \cdot cm^2$. By introducing the corrosive gases, Q_{dl} of the steel increases, which indicates that the surface of electrode become inhomogeneous; R_{ct} and R_f decreases obviously suggesting that the corrosion resistance of steel passive films are deceased. The polarization resistance R_p ($R_p = R_{ct} + R_f$) is often used to evaluate the corrosion resistance of materials [17,18], the greater R_p values, the higher corrosion resistance of the material. As shown in Table 1, the R_p values of the steel decreases with the introducing the corrosive gases revealing that the corrosion resistance of FV520B steel decreases with the CO_2 or H_2S filling into the SW, which is consistent with the previous OCP testing results.

Table 1. The electrochemical parameters of FV520B steel after immersion in different salinity solutions obtained from the EIS curves.

Environment	R_s, $\Omega \cdot cm^2$	R_{ct}, $\Omega \cdot cm^2$	Q_{dl}, Y_0 ($\times 10^{-6}$) $\Omega^{-1} \cdot cm^{-2} \cdot s^n$	n	R_f, $k\Omega \cdot cm^2$	Q_f, Y_0 ($\times 10^{-6}$) $\Omega^{-1} \cdot cm^{-2} \cdot s^n$	n
SW	4.76	1360	31.1	0.98	41.86	78.1	0.58
SW+CO_2	3.72	1104	31.8	0.99	26.75	103.3	0.59
SW+H_2S	3.33	508	92.8	0.94	12.44	149.7	0.56

3.3. Polarization curve

The polarization curves of FV520B steel after immersion in salinity solutions are presented in Fig. 4. It is clear that all curves show the typical passivation behavior. Additionally, the self−corrosion potential (E_{corr}) of the steel exhibit the same changing trend as the OCP, which becomes more negative with the introducing of CO_2 or H_2S into the SW. E_{corr} is the corresponding potential when the current density is zero, where the number of electrons in the cathodic is equal to that in the anodic reaction [19]. Although the variation trend of OCP is consistent with that of E_{corr}, OCP is measured without external current. With the introducing corrosive gases, the polarization curve moves to the right, which indicates that the corrosion rate increases with the filling CO_2 or H_2S.

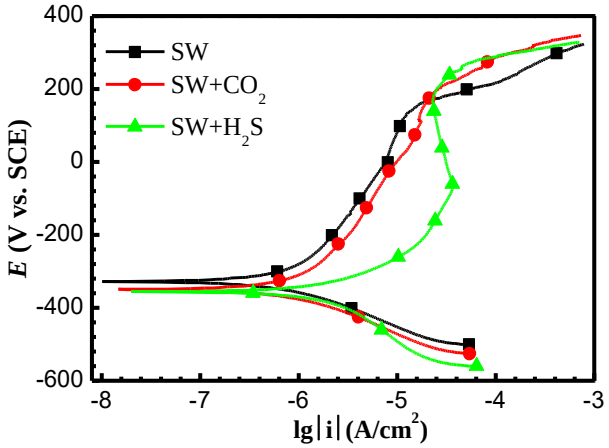

Figure 4. Polarization curves of FV520B steel after immersion in different salinity solutions.

According to the relationship between the current density *i* and the polarization potential *E* of the Butter−Volmer equation [13,20].

$$i = i_{\text{corr}}[\exp(2.303\Delta E)/b_a - \exp(-2.303\Delta E)/b_c], \quad 1)$$

$$\Delta E = E - E_{corr}, \quad 2)$$

Where i_{corr} is the corrosion current density, b_a is the anode Tafel constant, and b_c is the cathode Tafel constant. b_a, b_c and i_{corr} can be calculated by a iterative fitting program, and the polarization resistance R_p and corrosion rate v are calculated by Eqs. (3) and (4) [13,20].

$$R_p = \frac{b_a b_c}{2.303(b_a + b_c) i_{\text{corr}}}, \quad 3)$$

$$v = 0.327 \frac{M i_{\text{corr}}}{n\rho} \quad 4)$$

Where the atomic weight *M* is 56 for the steel, the density of metal ρ is 7.87 g/cm^3, the electrode reaction *n* is 2, and the unit of i_{corr} is μA/cm^2.

The electrochemical parameters obtained from fitting the polarization curve data are shown in Table 2. As the CO_2 and H_2S was introducing into the salinity solutions, the i_{corr} increase from 0.189 to 0.293 and 0.705 μA/cm^2 respectively, indicating that the FV520B steel passive properties are seriously effected by the introducing of CO_2 and H_2S. The b_a are greater than that of absolute values of b_c, indicating that the anode is the control step of the whole electrochemical reaction.

Table 2. The electrochemical parameters of FV520B steel after immersion in different salinity solutions obtained from the polarization curves.

Environment	E_{corr}, mV	b_a, mV/dec	b_c, mV/dec	i_{corr}, μA/cm^2	*v*, μm/a
Salinity	−328	268	−122	0.189	2.217
Salinity+CO_2	−348	300	−128	0.293	3.437
Salinity+H_2S	−355	232	−147	0.705	8.270

3.4. Cyclic voltammetry curve

The fifth circles CV curves of the FV520B steel after immersion in salinity solutions are presented in Fig. 5. As can be seen from the CV curve, there is no obvious redox peak. With the introducing CO_2 and H_2S, the anode current density of forward sweep curve of CV increases, and the anode current density in H_2S salinity solution is the largest. When scanning to $-0.15V_{SCE}$, there is an oxidation peak 'A', which may indicate the behavior of passive film formation. Also, this peak may reflect the conversion between Fe^{2+} and Fe^{3+} [21,22]. The current density i_{0V} is the corrosion resistance index of passive film [23], generally, the higher i_{0V}, the worse the corrosion resistance of passive film and the greater the corrosion probability of steel. From the CV curve, it can be seen that the i_{0V} of FV520B steel in SW, SW+CO_2 and SW+H_2S solutions are 29.1, 34.3 and 65.6 μA/cm^2 respectively, which further indicate that the corrosion resistance of steel decreases with the introducing of CO_2 and H_2S, and the corrosion resistance of steel is the worst in SW+H_2S solution.

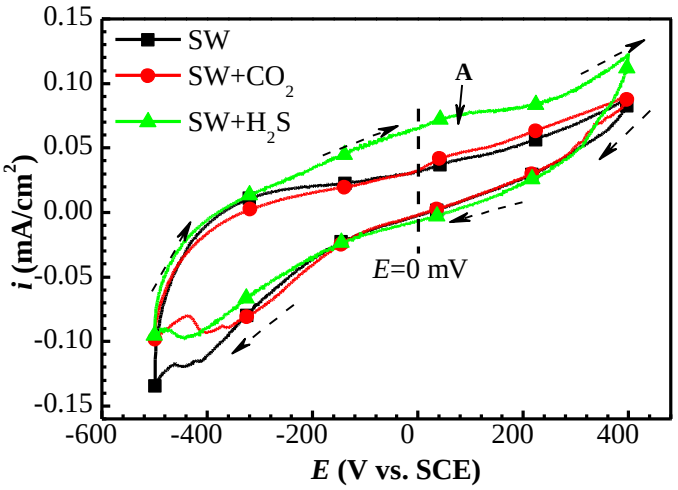

Figure 5. Cyclic voltammetry curves of FV520B steel after immersion in different salinity solutions.

3.5. Passive film composition

The passive film chemical composition may have great effects on the corrosion resistance of FV520B steel. Base on the binding energy of steel (Table 3), the major oxides of FV520B steel passive film after immersion in different salinity solutions for 1 day are assessed by XPS. As is shown in Figs. 6− 12, all the metallic and oxidized states of Fe $2p_{3/2}$, Cr $2p_{3/2}$, Mo 3d, Ni $2p_{3/2}$, Cu $2p_{3/2}$ and O1s are all presented (Fig 6). Binding energy shift was observed mainly in Fe $2p_{3/2}$, Cr $2p_{3/2}$, Mo 3d, and O 1s profiles indicating changes in the passive film composition with the CO_2 and H_2S introducing into the salinity solution [24].

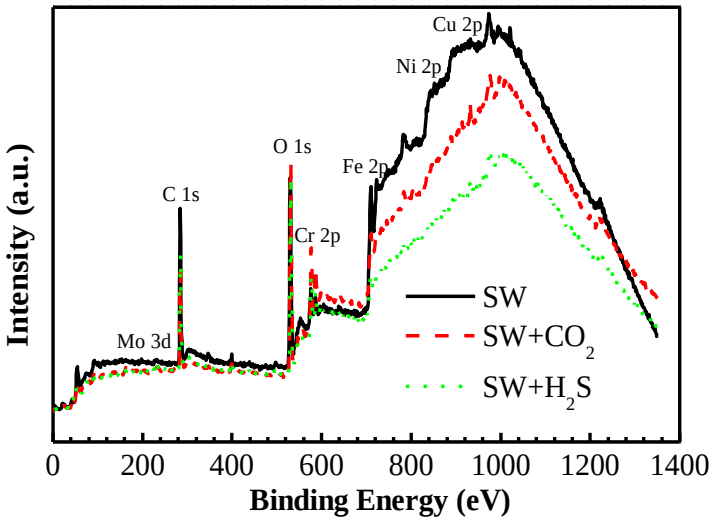

Figure 6. XPS peak of the survey scan spectra obtained form the passive of FV520B steel after immersion in different salinity solutions for 1 day.

Table 3. The binding energy of major oxides of FV520B steel passive film after immersion in different salinity solutions for 1 day.

Element	Peak	Species/binding energy (eV)
Fe	$2p_{3/2}$	$Fe_{(met)}$/706.7; FeO /709.4; Fe_2O_3 /710.9;FeOOH /711.8
Cr	$2p_{3/2}$	$Cr_{(met)}$ /574.1; Cr_2O_3 /576.3; $Cr(OH)_3$ /577.1; Cr(VI) /578.7
Mo	$3d_{5/2}$	$Mo_{(met)}$ /227.4; Mo^{4+} /230.2; Mo^{6+} /232.2
	$3d_{3/2}$	$Mo_{(met)}$ /230.9; Mo^{4+} /233.4; Mo^{6+} /235.1
Ni	$2p_{3/2}$	$Ni_{(met)}$ /852.8; $Ni(OH)_2$ /855.6; Ni_2O_3/856
Cu	$2p_{3/2}$	$Cu_{(met)}$ and Cu_2O /932.5
O	1S	O^{2-}/530.2; OH^-/531.8; H_2O/533

It is clearly in Fig. 7, the iron profile showed mainly four peaks: $Fe_{(met)}$ (706.7 eV), FeO (709.4 eV),Fe_2O_3 (710.9 eV) and FeOOH (711.8 eV). From the peak intensity of Fe^{2+} and Fe^{3+} in XPS, it can be concluded that the passive films of FV520B steel in three salinity solutions are mainly composed of oxides and hydroxides of Fe^{3+}. $Fe_{(met)}$ could be detected, indicating that the thickness of passive film should be about several nanometers [25,26]. With the introducing of CO_2 and H_2S into the SW, the peak intensity of $Fe_{(met)}$ becomes wider, which indicates that the thickness of passive film decreases and the corresponding corrosion resistance decreases. The oxides of Fe^{2+} in passive film are recognized to have good corrosion resistance and the content of Fe^{2+} also decreases with the introducing of corrosive gases [16]. The XPS results shows that the corrosive gases promotes the oxidation process of Fe^{2+} to Fe^{3+}, thus reducing the corrosion resistance of FV520B steel passive film.

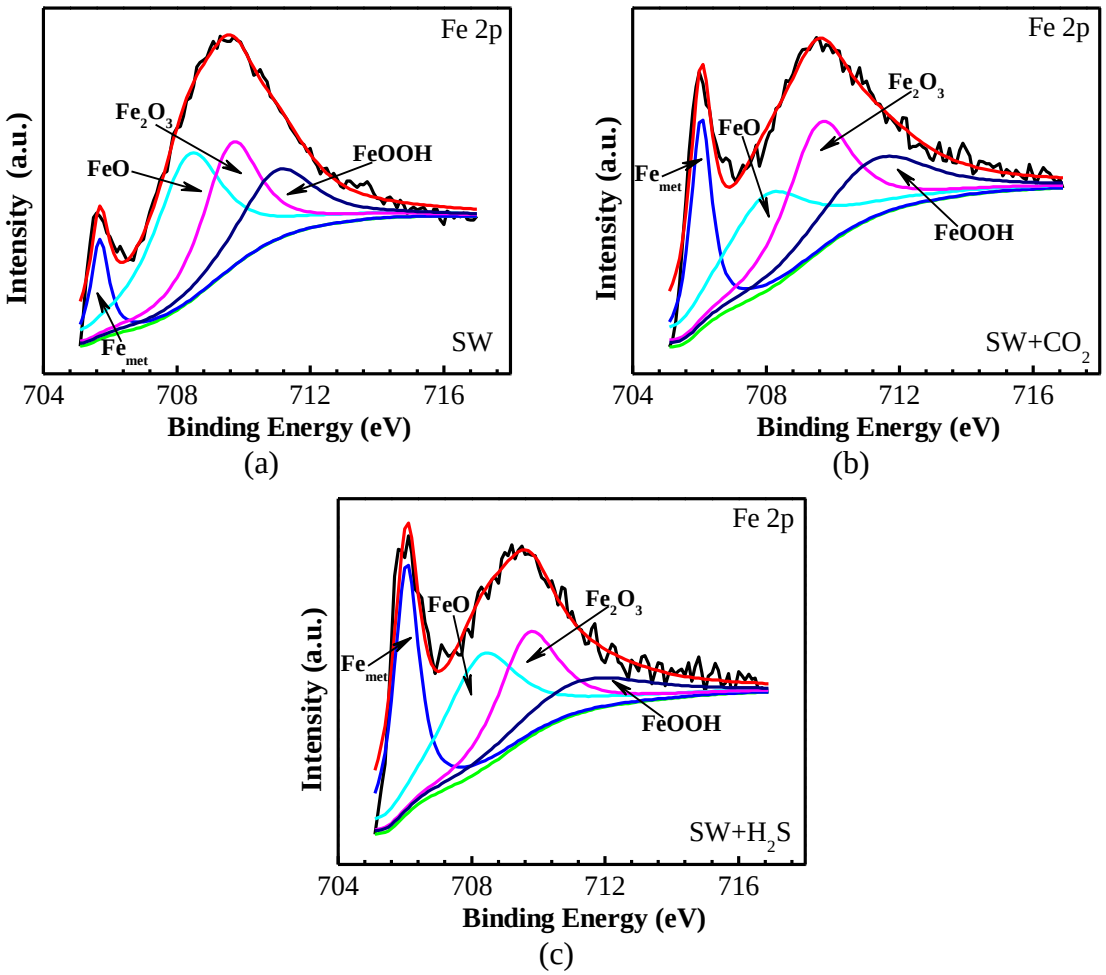

Figure 7. XPS peak of Fe2p peaks obtained form the passive of FV520B steel after immersion in different salinity solutions for 1 day: (a) SW; (b) SW+CO_2 ; (c)SW+H_2S.

The Cr 2p peaks obtained form the passive of FV520B steel after immersion in different salinity solutions for 1 day are shown in Fig. 8, the chromium profile showed mainly three peaks: $Cr_{(met)}$ (574.1 eV), Cr_2O_3 (576.3 eV) and Cr $(OH)_3$ for FV520B steel in salinity water and four peaks: $Cr_{(met)}$ (574.1 eV), Cr_2O_3 (576.3 eV), Cr $(OH)_3$ (577.1 eV) and CrO_3 (578.7 eV) for the steel in corrosive gases containing solutions. As the CO_2 and H_2S were filled into the SW, the intensity of CrO_3 is much higher compared to the steel in SW and the intensity of $Cr(OH)_3$ is less. The Cr^{3+} is the key elementary substance to self−repairing and maintaining stability of passive film of stainless steel [27]. Therefore, the passive film of FV520B steel in SW has higher stability.

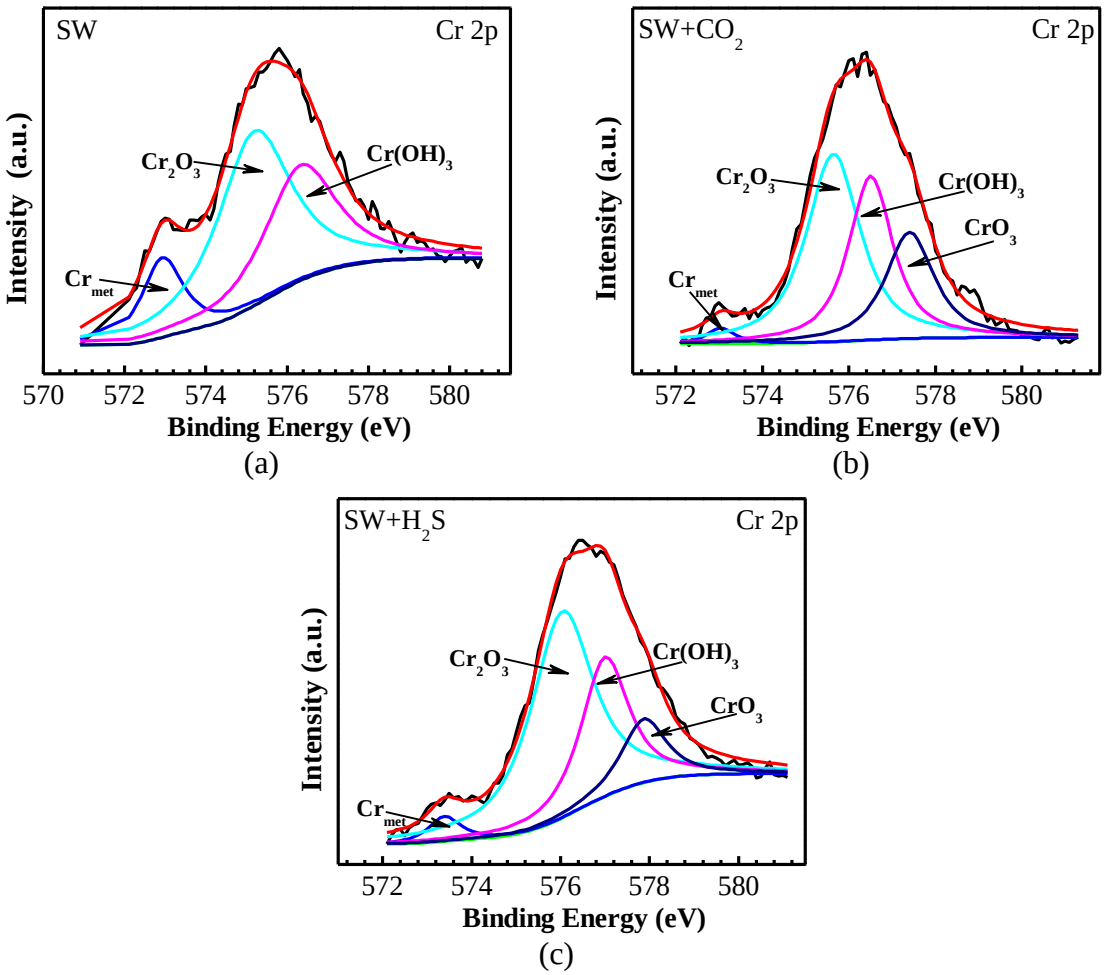

Figure 8. XPS peak of Cr 2p peaks obtained form the passive film of FV520B steel after immersion in different salinity solutions for 1 day: (a) SW; (b) SW+CO_2; (c)SW+H_2S.

The Mo 3d peaks of the passive film of FV520B steel after immersion in different salinity solutions for 1 day are shown in Fig. 9. The Mo 3d spectra can be divided into six peaks: Mo $3d_{5/2}$ (227.4 eV), Mo^{4+} $3d_{5/2}$ (230.2 eV), Mo^{6+} $3d_{5/2}$ (232.2 eV), Mo $3d_{3/2}$ (230.9 eV), Mo^{4+} $3d_{3/2}$ (233.4 eV) and Mo^{6+} $3d_{3/2}$ (235.1 eV). It can be seen that Mo 3d spectra of FV520B steel passive film in SW with or without corrosive gases are different. In SW, the hexa−valent (Mo^{4+}) is the main species in the passive film. However, after introducing corrosion gases to SW, the hexa−valent (Mo^{6+}) is the main species in the passive film. It is well known that Mo^{6+} may be attributed to $Fe_2(MoO_4)_3$ or MoO_3 species in stainless steel passive film [28,29]. Thus, it can be deduced that the Mo 3d spectra of passive films in SW, SW+CO_2 and SW+H_2S solutions are different.

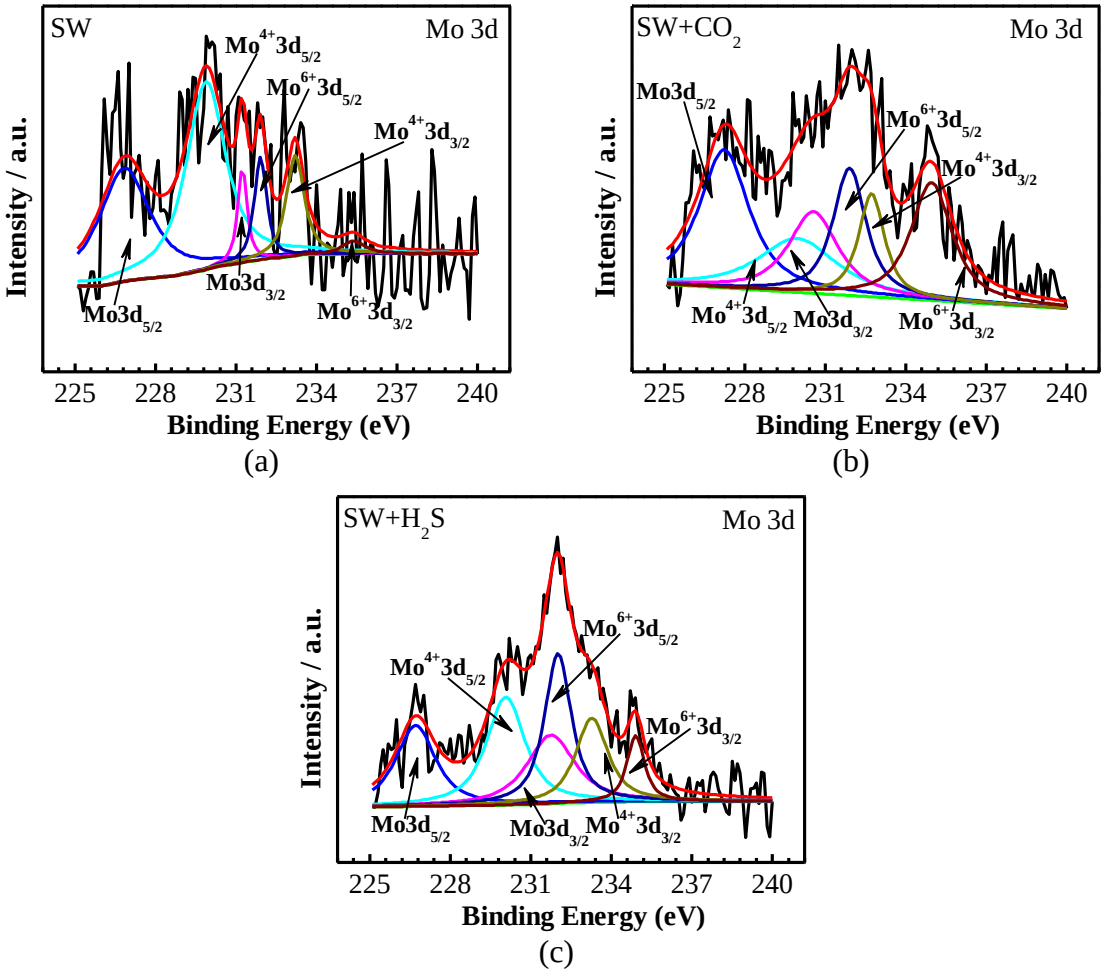

Figure 9. XPS peak of Mo3d peaks obtained form the passive film of FV520B steel after immersion in different salinity solutions for 1 day: (a) SW; (b) SW+CO_2 ; (c)SW+H_2S.

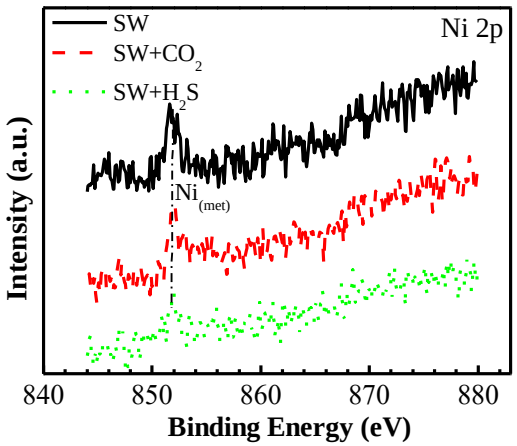

Figure 10. XPS peak of Ni2p peaks obtained form the passive film of FV520B steel after immersion in different salinity solutions for 1 day.

The Ni 2p peaks of the passive film of FV520B steel after immersion in different salinity solutions for 1 day are shown in Fig. 10, the Ni $2p_{3/2}$ spectra exhibit that the intensity of nickel is strongest

in the salinity solution and slightly decreases as the CO_2 and H_2S are introduced. It is reported that the passive film growth and its corrosion resistance were influenced by the presence of nickel [30]. Nickel also has a great influence on the distribution of Cr element in passive film, thus, the FV520B steel show good corrosion resistance in SW without introducing corrosive gases.

The Cu 2p peaks of the passive film of FV520B steel after immersion in different salinity solutions for 1 day are shown in Fig. 11. The spectra represented peaks corresponding to $Cu_{(met)}$ and Cu_2O (932.5 eV). Due to the binding energies of $Cu_{(met)}$ and Cu_2O are very close (932.5 eV), it is impossible to distinguish them, the findings are in accords with other XPS findings of higher Cu content stainless steel [31]. With the introducing corrosive gases into the SW, the intensity peak of Cu increases, and the passive film formed in the SW+ CO_2 solution shows the highest.

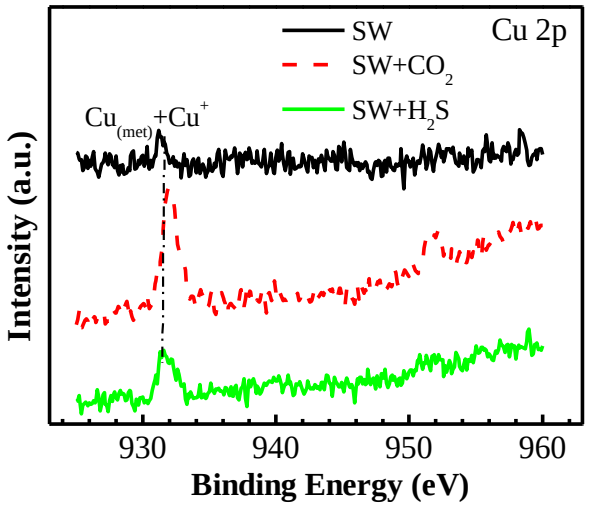

Figure 11. XPS peak of Cu2p peaks obtained form the passive film of FV520B steel after immersion in different salinity solutions for 1 day.

The O 1s peaks of the passive film of FV520B steel after immersion in different salinity solutions for 1 day are shown in Fig. 12, the oxygen profile showed mainly two peaks: O^{2-} (530.2 eV) and OH^- (531.8 eV) for FV520B steel in SW and three peaks: O^{2-}(530.2 eV), OH^-(531.8 eV) OH^- and H_2O (533 eV) for the passive films in corrosive gases containing solutions. Oxygen plays a major role in binding metal ions in passive films. It can be seen from the Fig. 12 that the passive film contains more OH^-, which is consistent with the formation of $Cr(OH)_3$ and FeOOH. While O^{2-} is also the basic composition of the passive film, which corresponds to the formation of FeO, Fe_2O_3 Cr_2O_3, MoO_3 and CuO.

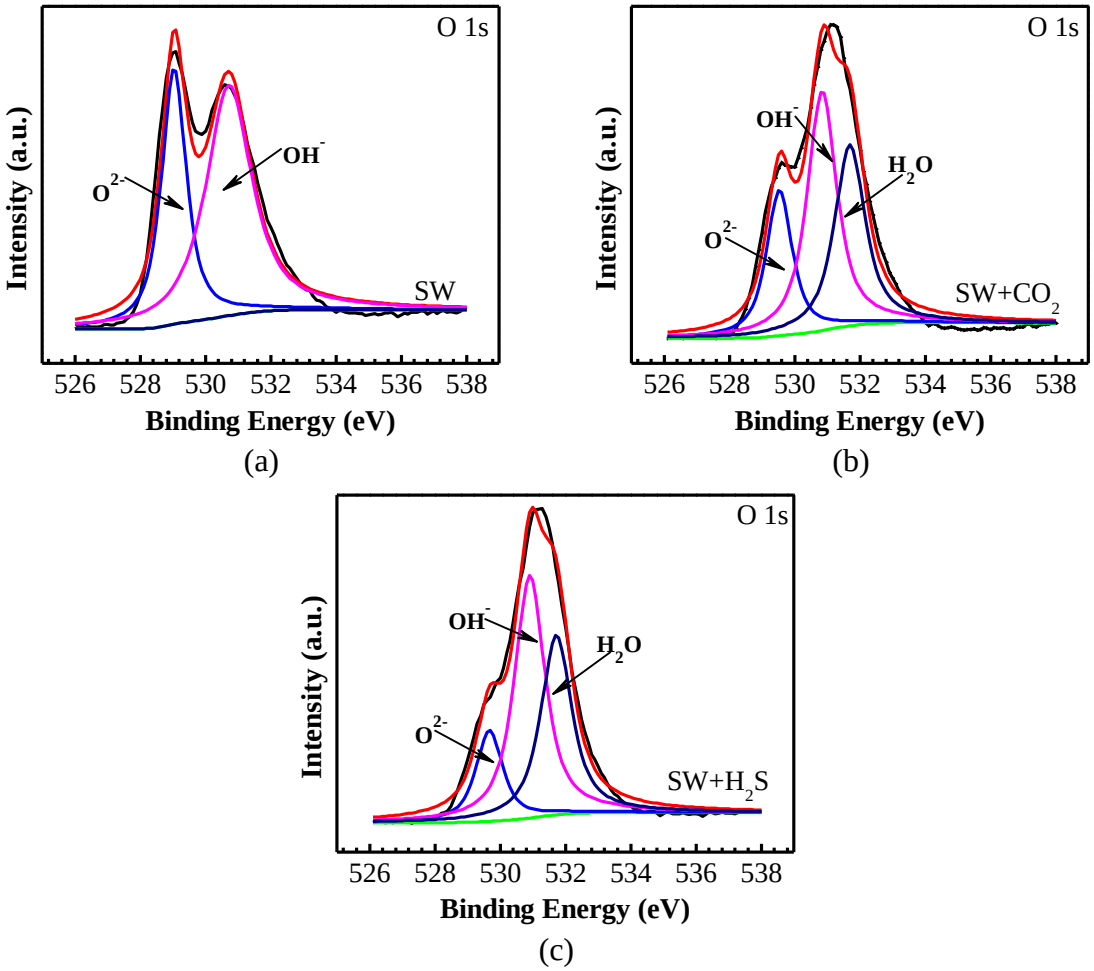

Figure 12. XPS peak of O1s peaks obtained form the passive film of FV520B steel after immersion in different salinity solutions for 1 day: (a) SW; (b) SW+CO_2 ; (c) SW+H_2S.

4. CONCLUSIONS

1. The introduction of corrosive gases CO_2 and H_2S into SW obviously increases the corrosion tendency of FV520B steel, the order of thermodynamic stability of FV520B steel in three test salinity solutions are: SW > SW+ CO_2 > SW+ H_2S.

2. FV520B steel show typical passivation behavior in different salinity solutions. With the introducing of corrosive gases, the polarization curve moves to the right, the corrosion current density increases, the polarization resistance decreases, and the corrosion resistance shows the worst in SW+ H_2S solution.

3. Based on the XPS analysis, the major passive film of FV520B steel formed in salinity solutions, the primary compounds of passive film are Fe, Cr, Mo, Ni and Cu oxides. Nevertheless, the content of the Fe, Cr, Mo and Ni oxides changed in the different salinity solutions.

ACKNOWLEDGMENTS
The authors gratefully acknowledge the financial supports from National Natural Science Foundation of China (Project 51801149), the China Postdoctoral Science Foundation (Project 2017M620448) and Fund of State Key Laboratory for Strength and Vibration of Mechanical Structures (Project SV2019-KF-10).

CONFLICTS OF INTEREST
The authors declare no conflict of interest.

References

1. G. Fayaz, S. Kazemzadeh, 3D Print. *Addit. Manuf.*, 20 (2018) 182.
2. S. J. Luo, M. Liu, N. H. Wen, Y. Shen, Y. M. Liu, X.Z. lin, *Int. J. Electrochem. Sci.*, 14 (2019) 2589.
3. R. Derakhshandeh−Haghighi, *J Fail. Anal. and Preven.*, 17 (2017) 522.
4. M. Qin, J. Li, S. Chen, Y. Qu, *Results. Phys.*, 6 (2016) 365.
5. Y. Zhang, B. Xu, H. Wang, P. He, Z. Xing, B. Fan, *Eng. Fail. Anal.*, 59 (2016) 111.
6. M. Zhang, W.Wang, P. Wang, Y. Liu, J. Li, *Eng. Fail. Anal*., 66 (2016) 432.
7. Y. Sui, C. Sun, J. Sun, B. Pu, W. Ren, W. Zhao, *Materials*., 10 (2017) 632.
8. M. Liu, S. J. Luo, Y. Shen, X. Z. Lin, *Eng. Fail. Anal.*, 97 (2019) 493.
9. Q. Chu, M. Zhang, J. Li, *Eng. Fail. Anal.*, 34 (2013) 501.
10. D. Nie, X. Chen, Z. Fan, Q. Wu, *Eng. Fail. Anal.*, 42 (2014) 1.
11. F. Fantechi, M. Innocenti, *Eng. Fail. Anal.*, 8 (2001) 477.
12. J. Wang, Y. Zhang, S. Liu, Q. Sun, H. Lu, *Int. J. Fatigue.*, 87 (2016) 203.
13. R. Wang, S. Luo, M. Liu, Y. Xue, *Corros. Sci.*, 85 (2014) 270.
14. Y. Pan, X. Kui, C. Dong, K. Ding, M. Liu, X. Li, Int. *J. Electrochem. Sci.*, 10 (2015) 7754.
15. M. Liu, X. Cheng, G. Zhao, X. Li, Y. Pan, *Surf. Interface Analysis.*, 48 (2016) 981.
16. M. Liu, X. Cheng, X. Li, Y. Pan, J. Li, *Appl. Surf. Sci.*, 389 (2016) 1182.
17. N. K. Liyana, M. A. Fazal, A. S. M. A. Haseeb, *Mater. Sci.−Poland.*, 35 (2018) 694.
18. M. Liu, X. Cheng, X. Li, T. Lu, *J Electroanal. Chem.*, 803 (2017) 40.
19. X. Huang, J. Xu, J. *Zhejiang Univ.Sci A.*, 14 (2013) 292.
20. M. Liu, X. Cheng, X. Li, C. Zhou, H. Tan, *Constr. Build. Mater.*, 130 (2017) 193.
21. J. M. Deus, L. Freire, M. F. Montemor, X. R. Nóvoa, *Corros. Sci.*, 65 (2012) 556.
22. L. Veleva, M. A. Alpuche−Aviles, M. K. Graves−Brook, D. O. Wipf, *Electroanal. Chem.*, 578 (2005) 45.
23. J. Shi, W. Sun, G. Geng, *Acta. Metall. Sin.*, 47 (2011) 17.
24. H. Luo, X. Li, C. Dong, K. Xiao, Surf. Interface Anal., 45 (2013) 793.
25. L. Freire, M. A. Catarino, M. I. Godinho, M. J. Ferreira, M. G. S. Ferreira, A. M. P. Simões, M. F. Montemor, *Cement. Concrete Comp.*, 34 (2012) 1075.
26. H. Luo, H. Su, C. Dong, K. Xiao, X. Li,, *Constr. Build. Mater.*, 96 (2015) 502.
27. M. G. Faichuk, S. Ramamurthy, W. M. Lau, *Corros. Sci.*, 53 (2011) 1383.
28. H. Luo, C. Dong, K. Xiao, X. Li, *J. Mater. Eng. Perform.*, 26 (2017) 2237.
29. T. J. Mesquita, E. Chauveau, M. Mantel, R. P. Nogueita, *Appl. Surf. Sci.*, 270 (2013) 90.
30. C. M. Abreu, M. J. Cristóbal, R. Losada, X. R. Nóvoa, G. Pena, M. C. Pérez, *Electrochim. Acta.*, 51 (2006) 2991.
31. H. T. Lin, W. T. Tsai, J. T. Lee, C. S. Huang, *J. Cheminformatics.*, 33 (1992) 691.